A Solid-State ^{17}O NMR Study of L-Tyrosine in Different Ionization States: Implications for Probing Tyrosine Side Chains in Proteins

Jianfeng Zhu, Justin Y. C. Lau, and Gang Wu*

Department of Chemistry, Queen's University, 90 Bader Lane, Kingston, Ontario, Canada K7L 3N6

Received: June 15, 2010; Revised Manuscript Received: July 30, 2010

We report experimental characterization of ^{17}O quadrupole coupling (QC) and chemical shift (CS) tensors for the phenolic oxygen in three L-tyrosine (L-Tyr) compounds: L-Tyr, L-Tyr·HCl, and Na_2(L-Tyr). This is the first time that these fundamental ^{17}O NMR tensors are completely determined for phenolic oxygens in different ionization states. We find that, while the ^{17}O QC tensor changes very little upon phenol ionization, the ^{17}O CS tensor displays a remarkable sensitivity. In particular, the isotropic ^{17}O chemical shift increases by approximately 60 ppm upon phenol ionization, which is 6 times larger than the corresponding change in the isotropic ^{13}C chemical shift for the C^{ζ} nucleus of the same phenol group. By examining the CS tensor orientation in the molecular frame of reference, we discover a "cross-over" effect between δ_{11} and δ_{22} components for both ^{17}O and ^{13}C CS tensors. We demonstrate that the knowledge of such "cross-over" effects is crucial for understanding the relationship between the observed CS tensor components and chemical bonding. Our results suggest that solid-state ^{17}O NMR can potentially be used to probe the ionization state of tyrosine side chains in proteins.

1. Introduction

The importance of the element oxygen in organic and biological molecules cannot be overstated. In recent years, considerable effort has been devoted to the development of solid-state ^{17}O NMR spectroscopy for direct detection of oxygen nuclei in biologically important molecules.[1,2] To date, ^{17}O quadrupole coupling (QC) and chemical shift (CS) tensors have been experimentally characterized for many oxygen-containing organic functional groups including carboxylic acids,[3−6] amino acids,[7−13] polypeptides,[14−19] nucleobases,[20−22] nucleosides,[23] amides,[24,25] urea,[26] ketones,[27] aldehydes,[27,28] α-keto acids,[29] carbohydrates,[30] and *C*-nitrosoarenes.[31] Very recently, we have successfully detected solid-state ^{17}O NMR signals in large protein−ligand complexes of size on the order of 40 kDa per ligand.[32] Despite these significant advances, there are still important functional groups for which the relevant ^{17}O NMR tensors have remained unknown. As part of our ongoing program in measuring ^{17}O NMR tensors in organic and biological molecules, herein we report a solid-state ^{17}O NMR study of three L-tyrosine (L-Tyr) compounds: L-Tyr, L-Tyr·HCl, and Na_2(L-Tyr). In each of these compounds, the phenolic oxygen under investigation is isotopically labeled by ^{17}O (35−40%). Our objective was to investigate how ^{17}O QC and CS tensors of the phenolic oxygens in these compounds depend on the ionization (protonation) state. The outcome of this study will have implications on potential applications of solid-state ^{17}O NMR spectroscopy as a new probe for monitoring the ionization state of tyrosine (Tyr) side chains in peptides and proteins, as shown in Figure 1.

The ionization equilibrium of Tyr side chains of proteins is known to be important in determining the orientation and dynamics of the Tyr side chains, thus playing a key role in the overall conformation and biological activity of proteins.[33−35] Several spectroscopic methods including fluorescence,[36,37] Fourier transform infrared (FT-IR),[33,34,38,39] and ultraviolet resonance Raman[40] have been used to probe the ionization state of Tyr side chains in proteins. For example, Sackett et al.[37] found that two of the Tyr residues in N^5-(L-1-carboxyethyl)-L-ornithine synthase from *Lactococcus lactis* exhibit pK_a values of 8.5, which is nearly two pK_a units lower than that of free Tyr in aqueous solution (p$K_a \approx 10$). On the other extreme, some Tyr residues in myoglobins were found to have p$K_a > 12.5$.[41] These examples illustrate the remarkable sensitivity of the ionization behavior of Tyr side chains toward local environment in proteins.

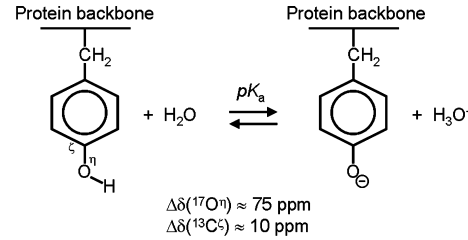

Figure 1. Ionization (acid−base) equilibrium of a tyrosine side chain.

In the context of NMR spectroscopy, solution ^{13}C NMR has been routinely used to monitor the titration process of Tyr residues in proteins.[41−43] In general, phenol ionization causes a ^{13}C chemical shift increase (shielding decrease) of approximately 10 ppm for C^{ζ}; see Figure 1.[44] Solid-state ^{13}C magic-angle spinning (MAS) NMR has also been used to probe the ionization state of Tyr residues in proteins.[45,46] In several cases, ^{13}C CS tensor components were also determined for C^{ζ}. Herzfeld and co-workers[45] reported that only the δ_{22} component of the ^{13}C CS tensor shows rather weak sensitivity toward phenol ionization. Because oxygen is at the center of a phenolic group, it is natural to consider ^{17}O NMR as a nuclear probe of this important functional group. In a pioneering ^{17}O NMR study, Eckert and Fiat[47] showed that the isotropic ^{17}O chemical shift of tyrosine is sensitive to phenol ionization with a titration chemical shift

* Corresponding author. E-mail: gang.wu@chem.queensu.ca.

10.1021/jp1055123
Published on Web 08/16/2010

increase of ca. 75 ppm on going from tyrosine to tyrosinate; see Figure 1. Clearly, this ^{17}O chemical shift change is much larger than the corresponding value observed for ^{13}C. Gerothanassis et al.[48] later confirmed these results. Boykin et al.[49] investigated the sensitivity of ^{17}O chemical shifts of phenols to hydrogen bonding interactions. Of course, these solution ^{17}O NMR studies did not yield complete information about the ^{17}O NMR tensors. In recent years, solid-state ^{17}O NMR has been used to characterize the ^{17}O NMR tensors in Tyr derivatives.[3,9,50] In particular, Dong et al.[3] reported the first set of solid-state ^{17}O NMR parameters for several phenols including DL-tyrosine. However, the quality of the reported spectra was generally poor; some key parameters such as ^{17}O chemical shift anisotropy need to be re-examined. Pike et al.[9] conducted a comprehensive solid-state ^{17}O NMR study of crystalline amino acids. For L-Tyr·HCl, they reported the following isotropic chemical shift (δ_{iso}), quadrupole coupling constant (C_Q), and asymmetry parameter (η_Q): $\delta_{iso} = 83$ ppm, $C_Q = 8.56$ MHz, and $\eta_Q = 0.65$. These parameters are slightly different from those observed by Brinkmann and Kentgens[50] for the same compound ($\delta_{iso} = 87.1$ ppm, $C_Q = 8.52$ MHz, and $\eta_Q = 0.74$). However, none of the two latter studies attempted to measure the ^{17}O CS tensor. Gervais et al.[51] used a plane-wave pseudopotential density functional theory (DFT) approach to compute ^{17}O QC and CS tensors for several amino acids including L-Tyr and L-Tyr·HCl. They found good agreement between experimental and computed NMR tensors for a variety of nuclei (^{13}C, $^{14/15}N$, ^{17}O, ^{35}Cl). In addition, Gullion and co-workers used L-[η-^{17}O]tyrosine to demonstrate $^{13}C-^{17}O$ rotational echo double resonance (REDOR) and rotational echo adiabatic passage double resonance (REAPDOR) NMR methods.[52,53] Brinkmann and Kentgens[54] showed that $^{1}H-^{17}O$ distances in L-Tyr·HCl can be measured using symmetry-based pulse sequences.

In this study, we obtained solid-state ^{17}O NMR spectra for L-Tyr, L-Tyr·HCl, and Na_2(L-Tyr) under both MAS and static conditions at three magnetic fields: 11.74, 14.09, and 21.14 T. Analysis of these MAS and static spectra allowed us to extract complete information about the ^{17}O QC and CS tensors for phenolic oxygens. Quantum chemical calculations were also performed to aid spectral analysis and to provide information about paramagnetic shielding contributions from the perspective of individual molecular orbitals (MOs). The observed ^{17}O NMR tensors for the phenolic oxygens of L-tyrosine and L-tyrosinate would lay the foundation for assessing the viability of solid-state ^{17}O NMR as a new probe for monitoring the ionization (protonation) state of Tyr side chains in peptides and proteins.

2. Experimental Section

Sample Preparation. L-Tyrosine (η-^{17}O, 35−40%) was purchased from Cambridge Isotope Laboratories (CIL) and directly used for solid-state ^{17}O NMR experiments without further purification. The hydrochloride salt of L-Tyr (L-Tyr·HCl) was prepared by dissolving L-Tyr in concentrated HCl(aq) solution (pH 0.5), followed by drying in air at room temperature. The chemical identities of the solid samples of L-Tyr and L-Tyr·HCl were checked by collecting ^{13}C CP/MAS NMR spectra; see the Supporting Information. All ^{13}C chemical shifts observed for both solid compounds were in excellent agreement with the literature values.[55,56] The sodium salt of L-Tyr, Na_2(L-Tyr), was prepared by dissolving L-Tyr in NaOH(aq) solution and adjusting the pH of the solution to 12.17. A solution ^{17}O NMR titration experiment was conducted to show that, at this pH, the phenolic oxygen of L-Tyr is fully ionized (deprotonated); see the Supporting Information. The solution of Na_2(L-Tyr) was then dried in air with a stream of N_2, and the solid sample was left in an oven at 60 °C for several hours.

Solid-State ^{17}O NMR. Solid-state ^{17}O NMR experiments of ^{17}O enriched L-Tyr, L-Tyr·HCl, and Na_2(L-Tyr) were performed on Bruker Avance-500 (11.74 T), Bruker Avance-600 (14.09 T), and Bruker Avance-II 900 (21.14 T) NMR spectrometers. A Hahn-echo sequence was used for both static and MAS experiments to eliminate the acoustic ringing from the probe. Effective 90° pulses of 1.9, 1.7, and 1.0 μs were used for the ^{17}O central-transition experiments at 11.74, 14.09, and 21.14 T, respectively. At 11.74 and 14.09 T, the ^{17}O MAS NMR spectra were performed using 4 mm Bruker MAS probes at spinning frequencies of 10−12 kHz. At 21.14 T, the ^{17}O MAS NMR spectra were obtained with a 3.2 mm Bruker MAS probe at spinning frequencies of 18−20 kHz. High power ^{1}H decoupling was applied in all experiments. A liquid H_2O sample was used for both RF power calibration and ^{17}O chemical shift referencing ($\delta = 0$ ppm). Solid-state ^{17}O NMR spectra were analyzed using WSOLIDS[57] and DMfit.[58]

Quantum Chemical Calculations. Quantum chemical calculations of ^{17}O QC and CS tensors were carried out on Sun Fire 25000 servers. Each of the servers is equipped with 72× dual-core UltraSPARC-IV + 1.5 GHz processors with 576 GB of RAM. For L-Tyr and L-Tyr·HCl, first-principles calculations were performed using the CASTEP (version 4.3) program.[59] The calculations were performed using ultrasoft pseudopotentials generated from the "on-the-fly" method[60] implemented within the CASTEP program and the GGA PBE exchange-correlation functional. A plane wave cutoff energy of 550 eV was used for both L-Tyr and L-Tyr·HCl. Monkhorst−Pack (MP) grids of 4 × 1 × 4 (corresponding to 4 k-points) and 2 × 3 × 5 (10 k-point) were applied in the calculations for L-Tyr and L-Tyr·HCl, respectively. The neutron diffraction crystal structures of L-Tyr and L-Tyr·HCl from the literature[61] were used without further modification. For Na_2(L-Tyr), because no crystal structure is available in the literature, we used a molecular model whose geometry was fully optimized at the B3LYP/6-311++G(d,p) level. Computations of ^{17}O QC and CS tensors in Na_2(L-Tyr) were performed using the Amsterdam Density Functional (ADF) software package.[62] The Vosko−Wilk−Nusair (VWN) exchange-correlation functional[63] was used for the local density approximation (LDA), and the Perdew−Burke−Ernzerhof (PBE) exchange-correlation functional[64] was used for the generalized gradient approximation (GGA). Standard Slater-type-orbital (STO) basis sets with triple-ζ quality plus polarization functions (TZP and TZ2P) were used for all of the atoms. The spin orbital relativistic effect was incorporated in some calculations via either the Pauli-type Hamiltonian[65] or the zero order regular approximation (ZORA).[66−69]

The calculated principal components of the electric-field-gradient (EFG) tensor (V_{XX}, V_{YY}, V_{ZZ}, where $|V_{XX}| \le |V_{YY}| \le |V_{ZZ}|$) were reported in atomic units, which can be related to the QC tensor components (χ_{XX}, χ_{YY}, χ_{ZZ}) in the following fashion: $\chi_{ii} = eV_{ii}Q/h \times 9.71736 \times 10^{21}$ (Hz). Very often, we define a quadrupole coupling constant (C_Q) and an asymmetry parameter (η_Q) according to the following definition: $C_Q = \chi_{ZZ} = eV_{ZZ}Q/h \times 9.71736 \times 10^{21}$ (Hz) and $\eta_Q = (V_{XX} - V_{YY})/V_{ZZ}$, where e is the elementary charge; Q is the nuclear quadrupole moment, $Q(^{17}O) = -2.558 \times 10^{-30}$ m^2;[70] and h is the Planck constant. The calculated shielding tensor components (σ_{11}, σ_{22}, σ_{33} where $\sigma_{11} < \sigma_{22} < \sigma_{33}$) were converted to the corresponding CS tensor components (δ_{11}, δ_{22}, δ_{33}) using the absolute ^{17}O shielding scale reported by Wasylishen and Bryce:[71] δ (ppm) = 287.5 (ppm) − σ (ppm).

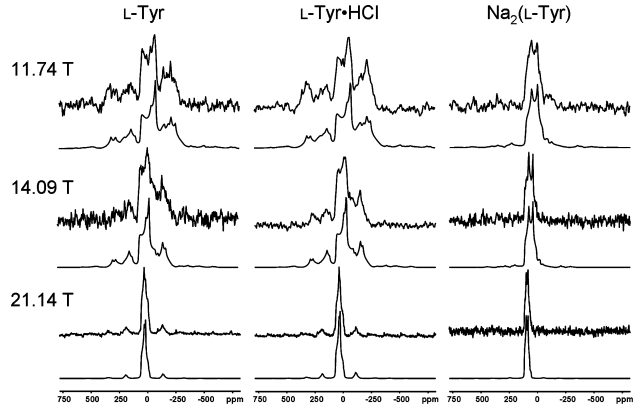

Figure 2. Experimental (upper trace) and calculated (lower trace) ^{17}O MAS NMR spectra of L-[^{17}O]tyrosine, L-[^{17}O]tyrosine•HCl, and Na_2(L-[^{17}O]tyrosinate). The detailed experimental parameters are as follows. L-[^{17}O]tyrosine: 11.74 T, 333 kHz spectral window, 12 kHz spinning, 20 s recycle delay, 2528 transients; 14.09 T, 333 kHz spectral window, 12 kHz spinning, 20 s recycle delay, 3754 transients; 21.14 T, 500 kHz spectral window, 20 kHz spinning, 20 s recycle delay, 12640 transients. L-[^{17}O]tyrosine•HCl: 11.74 T, 333 kHz spectral window, 12 kHz spinning, 5 s recycle delay, 5333 transients; 14.09 T, 333 kHz spectral window, 12 kHz spinning, 5 s recycle delay, 4121 transients; 21.14 T, 500 kHz spectral window, 18 kHz spinning, 5 s recycle delay, 12640 transients. Na_2(L-[^{17}O]tyrosinate): 11.74 T, 333 kHz spectral window, 12 kHz spinning, 2 s recycle delay, 26427 transients; 14.09 T, 333 kHz spectral window, 10 kHz spinning, 5 s recycle delay, 12328 transients; 21.14 T, 500 kHz spectral window, 18 kHz spinning, 2 s recycle delay, 12640 transients.

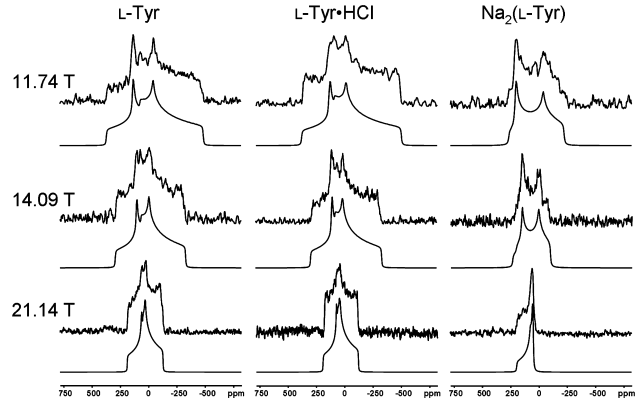

Figure 3. Experimental (upper trace) and calculated (lower trace) static ^{17}O NMR spectra of L-[^{17}O]tyrosine, L-[^{17}O]tyrosine•HCl, and Na_2(L-[^{17}O]tyrosinate). Detailed experimental parameters are as follows. L-[^{17}O]tyrosine: 11.74 T, 333 kHz spectral window, 20 s recycle delay, 3570 transients; 14.09 T, 333 kHz spectral window, 20 s recycle delay, 2465 transients; 21.14 T, 500 kHz spectral window, 20 s recycle delay, 6500 transients. L-[^{17}O]tyrosine•HCl: 11.74 T, 333 kHz spectral window, 5 s recycle delay, 7367 transients; 14.09 T, 333 kHz spectral window, 5 s recycle delay, 6557 transients; 21.14 T, 500 kHz spectral window, 5 s recycle delay, 12640 transients. Na_2(L-[^{17}O]tyrosinate): 11.74 T, 333 kHz spectral window, 2 s recycle delay, 29488 transients; 14.09 T, 333 kHz spectral window, 5 s recycle delay, 9535 transients; 21.14 T, 500 kHz spectral window, 2 s recycle delay, 28000 transients.

3. Results and Discussion

Spectral Analysis. Figure 2 shows the ^{17}O MAS NMR spectra of L-Tyr, L-Tyr•HCl, and Na_2(L-Tyr) obtained at three magnetic fields: 11.74, 14.09, and 21.14 T. In each spectrum, a typical line shape arising from second-order quadrupole interactions was observed for the ^{17}O central-transition (CT) NMR signal. As expected, the line width (in Hz) of the ^{17}O CT signal is scaled inversely with the applied magnetic field. At low magnetic fields, because the sample spinning frequency was comparable to the total line width of the CT signal, significant spinning sidebands were observed. This is particularly true for L-Tyr and L-Tyr•HCl, due to a combined effect of the QC and CS tensors (*vide infra*). At 21.14 T, in contrast, a clean line shape was observed in all three cases. For each compound, the ^{17}O MAS spectra obtained at three magnetic fields were analyzed *simultaneously*, which allowed us to obtain three important ^{17}O NMR parameters: δ_{iso}, $|C_Q|$, and η_Q. Then, we were able to use these results to further analyze the ^{17}O NMR spectra obtained for stationary powder samples at three magnetic fields, in order to obtain information about the ^{17}O CS tensor components and their relative orientations with respect to the ^{17}O QC tensor. As seen from Figure 3, the total line width of the ^{17}O static spectra generally decreases as the applied magnetic field is increased, suggesting that, in these compounds, the quadrupolar interaction is much larger than the chemical shift anisotropy. Once again, for each compound, a single set of NMR tensor parameters was used to simulate the static spectra at three magnetic fields simultaneously. In general, because static ^{17}O NMR spectra are sensitive to at least four adjustable tensor parameters, it is quite important to have multifield NMR data.[2] The final ^{17}O NMR tensor parameters obtained for L-Tyr, L-Tyr•HCl, and Na_2(L-Tyr) are summarized in Table 1, together with relevant literature data.

For L-Tyr, we observed that $\delta_{iso} = 81 \pm 1$, $|C_Q| = 8.5 \pm 0.1$ MHz, and $\eta_Q = 0.68 \pm 0.05$. Our analysis also yielded the following ^{17}O CS tensor components: $\delta_{11} = 129 \pm 5$, $\delta_{22} = 62 \pm 5$, and $\delta_{33} = 52 \pm 5$ ppm, which, to the best of our knowledge, is the first reliable ^{17}O CS tensor determined for a phenolic oxygen. The relative orientation of the ^{17}O CS tensor with respect to the QC tensor was determined to be $\alpha = 92 \pm 5°$, $\beta = 94 \pm 5°$, and $\gamma = 85 \pm 5°$. The definitions for the Euler angles (α, β, γ) can be found in one of our earlier publications.[25] For L-Tyr, we found that δ_{11} coincides nearly (within about 5°) with the smallest QC tensor component, χ_{XX}, whereas δ_{22} lies almost along the direction of the largest QC tensor component, χ_{ZZ}. Note that our analysis yielded only the relative orientations between the QC and CS tensors rather than the absolute tensor orientations in the molecular frame. As seen from Table 1, the CASTEP calculations are in reasonable agreement with the experimental results. It should be noted that our CASTEP results are in excellent agreement with those reported by Gervais et al.,[51] after taking into consideration the slightly different shielding scales used in the two studies.

For L-Tyr•HCl, we obtained that $\delta_{iso} = 87 \pm 1$, $|C_Q| = 8.5 \pm 0.1$ MHz, and $\eta_Q = 0.74 \pm 0.05$. These results are in excellent agreement with those reported by Brinkmann and Kentgens[50] but somewhat different from those reported by Pike et al.[9] We noticed, however, that the ^{17}O NMR parameters reported by Pike et al.[9] for L-Tyr•HCl are very similar to what we determined for L-Tyr; see Table 1. We have also determined the ^{17}O CS tensor components and their relative orientations for L-Tyr•HCl: $\delta_{11} = 127 \pm 5$, $\delta_{22} = 71 \pm 5$, and $\delta_{33} = 63 \pm 5$ ppm, $\alpha = 92 \pm 5°$, $\beta = 94 \pm 5°$, and $\gamma = 85 \pm 5°$. It is quite interesting to compare these parameters with those obtained for L-Tyr. The isotropic ^{17}O chemical shifts in these two compounds differ by 6 ppm, which is mainly due to the differences in δ_{22} and δ_{33}. The relative orientation between the ^{17}O CS and QC tensors is essentially the same in the two compounds. While the values of C_Q are identical in the two compounds, a slightly larger η_Q is observed for L-Tyr•HCl. This subtle difference in η_Q seems to be reproducible in several studies and thus deserves further investigation. Close examination of the crystal structures

TABLE 1: Experimental and Computed ^{17}O CS and QC Tensors for the Phenolic Oxygens in L-Tyrosine, L-Tyrosine Hydrochloride, and Na_2(L-Tyrosinate)[a]

compound	δ_{iso}/ppm	δ_{11}/ppm	δ_{22}/ppm	δ_{33}/ppm	C_Q[b]/MHz	η_Q	reference
			L-Tyr				
expt.	81 ± 1	129 ± 5	62 ± 5	52 ± 5	−8.5 ± 0.1	0.68 ± 0.05	this work
CASTEP	111	169	103	62	−8.8	0.66	this work
GIPAW[c]	85.0	142.9	80.3	31.8			51
			L-Tyr·HCl				
expt.	87 ± 1	127 ± 5	71 ± 5	63 ± 5	−8.5 ± 0.1	0.74 ± 0.05	this work
CASTEP	117	157	110	84	−8.70	0.82	this work
expt.	83				−8.56	0.65	9
GIPAW[c]	90.5	131.4	85.4	54.7			51
expt.	87.1				−8.52	0.74	50
BLYP/cluster[d]	87	125	79	57	−8.75	0.82	50
			Na_2(L-Tyr)				
expt.	140 ± 1	212 ± 5	178 ± 5	30 ± 5	−7.9 ± 0.1	0.46 ± 0.05	this work
ADF/TZP	120	190	184	−13	−8.6	0.61	this work

[a] The reported errors were estimated, from the spectra obtained at 21.14 T, by allowing the singularities observed in MAS and static spectra to vary within 100 and 500 Hz, respectively. [b] The sign of the experimental C_Q values was assumed to be the same as the computed ones. [c] This study used a slightly different ^{17}O shielding scale: $\delta = 261.5$ ppm $- \sigma$. [d] This study did not report the computed isotropic chemical shift. Here, CS tensor components were calculated assuming $\delta_{iso} = 87$ ppm.

of L-Tyr and L-Tyr·HCl determined by neutron diffraction experiments does reveal some structural differences in the hydrogen bonding environment around the phenolic oxygen atoms in the two compounds.[61] In both compounds, the phenolic oxygen atom serves simultaneously as a hydrogen bond donor and an acceptor. In L-Tyr, the phenolic oxygen atom is hydrogen bonded, as a donor, to an oxygen atom from $-COO^-$ of a neighboring L-tyrosine molecule with an $O^{\eta}\cdots O$ distance of 2.667 Å and an $O^{\eta}-H\cdots O$ bond angle of 173.76°. In L-Tyr·HCl, the phenolic oxygen atom is hydrogen bonded to Cl^- with an $O^{\eta}\cdots Cl$ distance of 3.045 Å and an $O^{\eta}-H\cdots Cl$ bond angle of 165.62°. These hydrogen bond distances can be considered to be of comparable strength, after taking into consideration the different atomic radii of O^{2-} and Cl^-.[72] When the phenolic oxygen atom is a hydrogen bond acceptor, however, a structural difference exists between these two compounds. In L-Tyr, the phenolic oxygen forms a hydrogen bond with N−H ($O^{\eta}\cdots H-N$ distance = 2.877 Å, $\angle O^{\eta}\cdots H-N = 129.8°$). In L-Tyr·HCl, on the other hand, the phenolic oxygen accepts a hydrogen from H−O ($O^{\eta}\cdots H-O$ distance = 2.619 Å, $\angle O^{\eta}\cdots H-O = 170.7°$). Apparently, the phenolic oxygen in L-Tyr·HCl is involved in an overall stronger hydrogen bonding environment. Indeed, the observed small differences in δ_{iso} and η_Q between these two compounds are consistent with the known relationships between ^{17}O NMR parameters and hydrogen bonding strength.[2] It is also important to note that the subtle differences between the experimental ^{17}O NMR parameters for these two compounds were quite well reproduced by the CASTEP calculations; see data shown in Table 1. Gervais et al.[51] carried out similar calculations for the ^{17}O CS tensors in L-Tyr·HCl, and our results are in good agreement with theirs. In comparison, Brinkmann and Kentgens[50] used a molecular cluster approach to compute ^{17}O NMR tensors in L-Tyr·HCl. Quite interestingly, their computational results from the largest cluster model (containing 10 molecules) are similar to those obtained with the crystal lattice approach (results presented in this study and those by Gervais et al.[51]); see data shown in Table 1. All of these computations suggest that the subtle differences in the ^{17}O NMR parameters observed between L-Tyr and L-Tyr·HCl are real and interpretable on the basis of hydrogen bonding strength.

In Na_2(L-Tyr), the phenolic group is ionized (deprotonated), representing the ionized (deprotonated) form of L-tyrosine. As a result, the ^{17}O NMR tensors observed for Na_2(L-Tyr) are significantly different from those seen in L-Tyr and L-Tyr·HCl. We have found the following parameters for Na_2(L-Tyr): $\delta_{iso} = 140 \pm 1$ ppm, $|C_Q| = 7.9 \pm 0.1$ MHz, $\eta_Q = 0.46 \pm 0.05$, $\delta_{11} = 212 \pm 5$, $\delta_{22} = 178 \pm 5$, $\delta_{33} = 30 \pm 5$ ppm, $\alpha = 0 \pm 5°$, $\beta = 90 \pm 2°$, and $\gamma = 0 \pm 5°$. This represents the first time that ^{17}O QC and CS tensors are measured for a phenol group in its ionized (deprotonated) state. Considering the fact that ^{17}O chemical shifts usually show large solvent effects, the isotropic ^{17}O chemical shift of 140 ppm observed for solid Na_2(L-Tyr) is in fair agreement with the previously reported ^{17}O chemical shift, 150.4 ppm, for the ionized (deprotonated) L-Tyr in aqueous solution.[48] The values of both C_Q and η_Q are smaller than those seen in L-Tyr and L-Tyr·HCl. The most striking change caused by phenol ionization was found to be in the ^{17}O CS tensor. For Na_2(L-Tyr), the span of the ^{17}O CS tensor ($\Omega = \delta_{11} - \delta_{33} = 182$ ppm) is more than doubled of those observed in L-Tyr (77 ppm) and L-Tyr·HCl (64 ppm). Furthermore, the relative orientations between the QC and CS tensors are also quite different. For Na_2(L-Tyr), δ_{11} lies along the direction of χ_{YY} and δ_{22} coincides with χ_{ZZ}. It is quite interesting to point out that, although all three compounds have similar C_Q values and Na_2(L-Tyr) exhibits a significantly larger chemical shift anisotropy, the static ^{17}O NMR spectrum of Na_2(L-Tyr) is actually 2 times *narrower* than those observed for L-Tyr and L-Tyr·HCl; see Figure 3. This trend is also consistent with the fact that significant spinning sidebands are observed in the MAS spectra of L-Tyr and L-Tyr·HCl but not in the spectrum of Na_2(L-Tyr) as noted earlier. This observation illustrates the important effect of tensor interplay on NMR line shapes, as noted by Wu et al.[28]

Because no crystal structure is available in the literature for Na_2(L-Tyr), it is impossible to perform similar CASTEP computations for this compound. To help shed some light on the general trends, we constructed an approximate model of Na_2(L-Tyr) using geometry optimization for a cluster containing a doubly ionized L-tyrosinate anion and two Na^+ ions, as shown in Figure 4. Because the pK_a values of L-tyrosine are 2.2 (−COOH), 9.1 ($-NH_3^+$), and 10.1 (−PhOH), the L-tyrosine molecules are doubly ionized under the experimental condition employed in this study (pH > 12). The calculated ^{17}O NMR tensors for this model are also listed in Table 1. Considering the approximate nature of the Na_2(L-Tyr) model, the qualitative

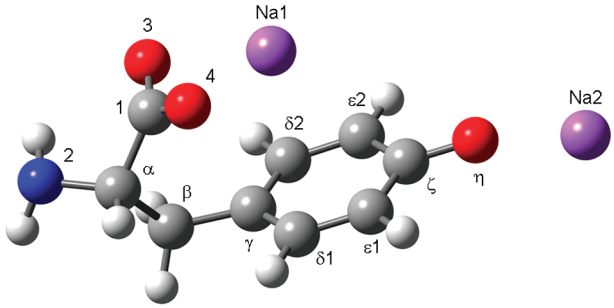

Figure 4. Molecular model of Na_2(L-Tyr) used in the quantum chemical calculations. The geometry of the model was fully optimized at the B3LYP/6-311++G(d,p) level. Selected bond lengths (Å) and bond angles (deg) are as follows: $O^{\eta}-C^{\zeta} = 1.306$, $C^{\zeta}-C^{\varepsilon 1} = 1.417$, $C^{\varepsilon 1}-C^{\delta 1} = 1.386$, $C^{\delta 1}-C^{\gamma} = 1.400$, $C^{\gamma}-C^{\beta} = 1.511$, $C^{\beta}-C^{\alpha} = 1.575$, $C^{\alpha}-N2 = 1.460$, $C^{\alpha}-C1 = 1.534$, $C1-O3 = 1.261$, $C1-O4 = 1.259$, $O^{\eta}-Na2 = 1.986$, $O3-Na1 = 2.308$, $O4-Na1 = 2.227$; $\angle O^{\eta}-C^{\zeta}-C^{\varepsilon 1} = 122.1$, $\angle O^{\eta}-C^{\zeta}-C^{\varepsilon 2} = 122.2$, $\angle O^{\varepsilon 1}-C^{\zeta}-C^{\varepsilon 2} = 115.8$, $\angle C^{\zeta}-C^{\varepsilon 1}-C^{\delta 1} = 121.9$, $\angle C^{\varepsilon 1}-C^{\delta 1}-C^{\gamma} = 122.1$, $\angle O3-C1-O4 = 124.7$.

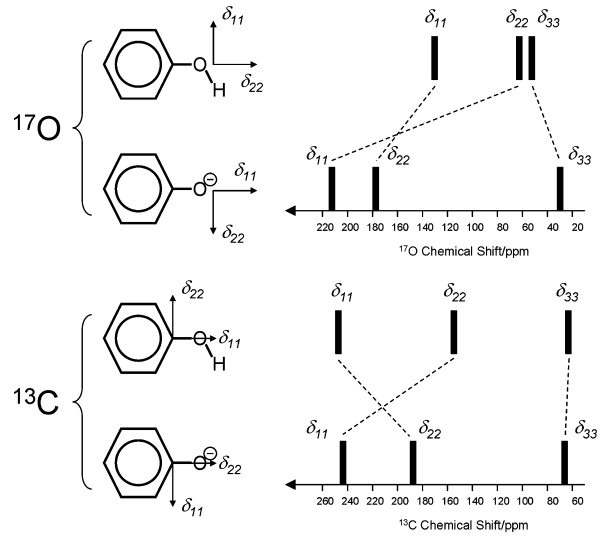

Figure 5. Illustration of the ^{17}O and ^{13}C CS tensor orientations in the molecular frame of reference and the $\delta_{11}-\delta_{22}$ "cross-over" effects observed between protonated and deprotonated phenol groups. The ^{13}C CS tensor components are from ref 45.

agreement between the computed and experimental ^{17}O NMR results shown in Table 1 is satisfactory. For the ^{17}O CS tensor orientation, the computation suggests that δ_{22} should lie along the direction of χ_{YY}, which is different from the experimental observation. However, it should be noted that the calculated δ_{11} and δ_{22} values differ by only 6 ppm. It is entirely possible that small structural modification of the current Na_2(L-Tyr) model shown in Figure 4 would lead to a switch in the directions of these two CS tensor components. This is indeed confirmed to be the case by computational results for a gas-phase phenolate anion as discussed later. Overall, the computation reproduces the general trends observed in the ^{17}O NMR parameters for Na_2(L-Tyr). From the results shown in Table 1, we can conclude that, while the ^{17}O QC tensor exhibits only small differences between the two phenol ionization states, the ^{17}O CS tensor is remarkably sensitive to the ionization nature of phenolic oxygens.

CS Tensor Orientations. In this section, we further examine the ^{17}O CS tensor orientations in the molecular frame of reference for phenolic oxygen atoms in different ionization states. All our quantum chemical calculations suggest that the ^{17}O QC tensor orientation is rather insensitive to weak molecular interactions and that it thus can be used as an internal reference. For protonated phenolic oxygen atoms (−PhOH), χ_{ZZ} is found to lie within the $C^{\zeta}-O^{\eta}-H$ plane and perpendicular to the directions of the electron lone pairs. This places χ_{XX} nearly bisecting the $C^{\zeta}-O^{\eta}-H$ angle. For ionized (deprotonated) phenolic oxygen atoms, χ_{ZZ} and χ_{XX} are perpendicular and parallel to the $C^{\zeta}-O^{\eta}$ bond, respectively. Coupling these absolute tensor orientations with the experimentally found relative orientation between QC and CS tensors, we can place the ^{17}O CS tensor into the molecular frame of reference. The results are shown in Figure 5. Because the ^{17}O CS tensors have different orientations in protonated and deprotonated phenol groups, it makes more sense to examine shielding changes along directions fixed to the molecular frame rather than to compare apparent changes in individual tensor components, $\Delta\delta_{11}$, $\Delta\delta_{22}$, and $\Delta\delta_{33}$. Such an analysis reveals that, upon phenol ionization, the shielding along the $C^{\zeta}-O^{\eta}$ bond direction decreases so much that this direction has the least shielding value (but the highest chemical shift value) and thus corresponds to the CS tensor component of δ_{11}, because the convention for defining the three CS tensor components is $\delta_{11} > \delta_{22} > \delta_{33}$. As a result, there is a "cross-over" between the δ_{11} and δ_{22} components upon phenol ionization if we link the CS tensor components according to their directions in the molecular frame, as depicted in Figure 5. The actual shielding change along the $C^{\zeta}-O^{\eta}$ bond direction is approximately 150 ppm, which is much larger than any of the $\Delta\delta_{ii}$ values. In fact, the overall change of ca. 60 ppm in δ_{iso}, upon phenol ionization, is primarily caused by the shielding change along the $C^{\zeta}-O^{\eta}$ bond direction, because the shielding changes in the other two orthogonal directions are nearly canceled by one another. This observation of orientation change in the ^{17}O CS tensor prompted us to consider the question of whether the ^{13}C CS tensor for C^{ζ} would exhibit the same behavior between the two phenol ionization states. Not too surprisingly, the quantum chemical calculations confirm that the ^{13}C CS tensor at C^{ζ} indeed exhibits a similar $\delta_{11}-\delta_{22}$ "cross-over" effect; see Figure 5. We should point out that, although the ^{13}C CS tensor components for L-tyrosine derivatives have been known for many years,[45,46,55,73−76] this CS tensor orientation switch at C^{ζ} upon phenol ionization has never been noticed before. It was, in fact, quite difficult to understand why only the δ_{22} component of the ^{13}C CS tensor displays weak sensitivity toward phenol ionization (an apparently drastic change in chemical bonding) as first observed by Herzfeld et al.[45] Now in light of this $\delta_{11}-\delta_{22}$ "cross-over" effect, the experimental observation of Herzfeld et al.[45] can finally be understood (*vide infra*).

Origin of the $\delta_{11}-\delta_{22}$ "Cross-Over" Effect. To fully understand the $\delta_{11}-\delta_{22}$ "cross-over" effects described in the previous section, we decided to use gas-phase phenol and phenolate molecules as computational models to further investigate shielding contributions from different molecular orbitals (MOs). In this context, our choice of phenol and phenolate was to simplify the analysis of MOs without losing generality. The B3LYP and MP2 optimized structures of phenol are within 3% of the experimental structures that were reported from electron diffraction and microwave spectroscopic studies;[77,78] see the Supporting Information. Although no experimental gas-phase phenolate structure is available in the literature, it can be inferred that, on the basis on the close agreement between optimized and experimental structures of phenol, the geometry optimization can give a reasonably accurate structure for a phenolate anion. Once we obtained the molecular structures, we used ADF to compute the shielding tensors, which were then converted to

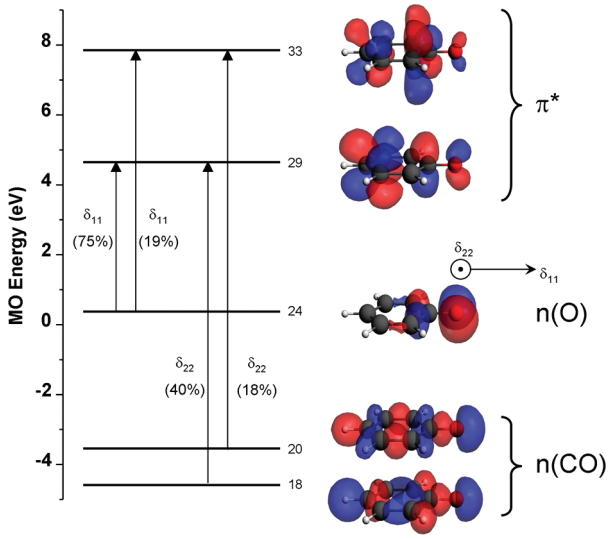

Figure 6. Selected occupied (#18, #20, and #24) and virtual (#29 and #33) MOs that have the largest paramagnetic shielding contributions at O^{η} in a phenolate anion. The percent paramagnetic shielding contribution (numbers in parentheses) is defined as the paramagnetic shielding contribution due to MO mixing along a particular direction over the total paramagnetic shielding contribution along the same direction.

CS tensors. More importantly, ADF also allows one to analyze paramagnetic shielding contributions from individual pairwise MOs. In principle, when one discusses paramagnetic shielding contributions, one refers to a shielding tensor rather than a CS tensor. However, to avoid the use of too many different symbols, we would discuss paramagnetic shielding contributions to individual CS tensor components (δ_{ii}) only in the context of the well-known relationship between the two quantities. That is, an increase in any CS tensor component along any direction would imply a decrease in shielding along the same direction. In the discussion that follows, such a decrease in shielding is very often caused by an increase in paramagnetic shielding contribution. The ADF results suggest that the largest MO contribution to the significant increase in paramagnetic shielding along the $C^{\zeta}-O^{\eta}$ bond upon phenol ionization is due to the presence of n(O) → π^* MO mixing, as illustrated in Figure 6. In comparison, the paramagnetic shielding contribution along the direction perpendicular to the $C^{\zeta}-O^{\eta}$ bond also increases upon phenol ionization, mainly resulting from n(CO) → π^* MO mixing. Here, n(CO) refers to the MO where the lone pair electrons are localized at the O atom but pointing along the C−O bond direction. It is well-known that the paramagnetic shielding contribution in Ramsey's shielding equations is inversely proportional to the energy gap between two mixing MOs.[79,80] Because the energy gap between n(CO) and π^* is much larger than that between n(O) and π^* MOs, the paramagnetic shielding increase is much larger along the $C^{\zeta}-O^{\eta}$ bond direction than perpendicular to it. Thus, δ_{11} lies along the $C^{\zeta}-O^{\eta}$ bond direction in the phenolate as opposed to being perpendicular to the $C^{\zeta}-O^{\eta}$ bond seen in a phenol, resulting in a $\delta_{11}-\delta_{22}$ "cross-over" effect as illustrated in Figure 5.

The situations for the ^{13}C CS tensors in phenol and phenolate are quite different from what have just been discussed for the ^{17}O CS tensors. In phenol, the δ_{11} component is nearly perpendicular to the $C^{\zeta}-O^{\eta}$ bond, primarily due to several MO mixings of n(O) → π^* nature, and δ_{22} is along the $C^{\zeta}-O^{\eta}$ bond with contributions from σ(CC) → π^* MO mixing. Upon phenol ionization, the energy gap between σ(CC) and π^* MOs is increased, resulting in a reduction in the paramagnetic shielding

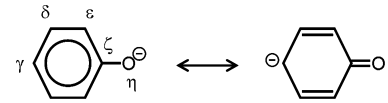

Figure 7. Resonance structures of a phenolate anion. Only the major quinone-type resonance structure is shown.

contribution along the $C^{\zeta}-O^{\eta}$ bond. In the direction perpendicular to the $C^{\zeta}-O^{\eta}$ bond, however, the paramagnetic shielding increases significantly because of the n(CO) → π^* MO mixing. As a result, the δ_{11} and δ_{22} components change in opposite directions, leading to an apparent "cross-over" or switch.

These $\delta_{11}-\delta_{22}$ "cross-over" effects can be readily understood on the basis of the resonance structures of the phenolate anion. As shown in Figure 7, one major resonance structure of the phenolate anion is the quinone-type structure. This is evidenced by several structural features of the phenolate anion. For example, the $C^{\varepsilon}-C^{\delta}$ bonds are substantially shorter than the $C^{\varepsilon}-C^{\zeta}$ bonds and the $C^{\zeta}-O^{\eta}$ bond has partial double bond character. In fact, the orientations of the ^{17}O QC, ^{17}O CS, and ^{13}C CS tensors for the $C^{\zeta}-O^{\eta}$ moiety of phenolate and of Na_2(L-Tyr) are identical to those found in carbonyl compounds such as ketones and aldehydes.[27,28,81−85]

At this point, it is also interesting to compare the sensitivity of the ^{17}O CS tensor toward phenol ionization with that of the ^{13}C CS tensor for C^{ζ}. It is important to note that, upon ionization, the δ_{11} and δ_{22} components of the ^{17}O CS tensor change in the same directions, whereas the corresponding components of the ^{13}C CS tensor change in opposite directions. As a result, the trace of the ^{17}O CS tensor, $\delta_{iso}(^{17}O)$, displays a change nearly 6 times larger than that in $\delta_{iso}(^{13}C)$. This increased sensitivity in ^{17}O NMR should be utilized as a new NMR probe for monitoring Tyr side chains in proteins.

Finally, although we have demonstrated that the ^{17}O NMR parameters are sensitive to the protonation state of the Tyr side chain, the issue whether this new solid-state ^{17}O NMR approach is practically feasible for studying proteins must be addressed. In this regard, there are two equally important aspects that deserve consideration. One is whether it is feasible to label the phenolic oxygen atoms of Tyr side chains by ^{17}O, and the other is whether the ^{17}O NMR sensitivity is sufficiently high to allow detection of weak signals. To address the first question, we note that the site-directed labeling methodology for introducing $^{13}C^{\zeta}$-labeled Tyr residues into peptides and proteins developed for FTIR studies[39] can be directly employed for introducing $^{17}O^{\eta}$-labeled Tyr residues into proteins for ^{17}O NMR studies. For the sensitivity issue, we have shown recently that high-quality solid-state ^{17}O NMR spectra can be obtained for large proteins (40 kDa per ^{17}O) at 21 T.[32] Here, the apparently poor signal-to-noise ratios obtained for three simple tyrosine compounds shown in Figures 2 and 3 are primarily due to the fact that the ^{17}O spin−lattice relaxation times (T_1) in these highly crystalline solids are very long and, as a result, long recycle times ranging from 2 to 20 s were used in acquiring the reported spectra. In our recent study,[32] however, we discovered that ^{17}O T_1 values in solid proteins are typically on the order of a few milliseconds (10^{-3} s). Therefore, rapid data acquisition (e.g., a recycle time of 30 ms), coupled with the use of other sensitivity enhancement methods, can routinely yield high-quality ^{17}O NMR spectra for proteins within a reasonable period of time.

4. Conclusions

We have experimentally determined the ^{17}O QC and CS tensors for phenolic oxygens in three L-tyrosine compounds:

L-Tyr, L-Tyr·HCl, and Na_2(L-Tyr). This is the first time that these fundamental ^{17}O NMR tensors are available for phenol groups in different ionization states. Our results suggest that phenol ionization of L-tyrosine results in only a small decrease in the absolute value of C_Q (from 8.5 to 7.9 MHz) but a significant change in CS tensor components. The largest change in shielding occurs along the $C^{\zeta}-O^{\eta}$ bond direction. We have discovered that phenol ionization also causes the ^{17}O and ^{13}C CS tensors to change their orientations in the molecular frame, resulting in a $\delta_{11}-\delta_{22}$ "cross-over" effect. Under such a circumstance, it is more informative to examine shielding changes along directions fixed to the molecular frame rather than apparent changes in individual CS tensor components, $\Delta\delta_{ii}$. Furthermore, we have shown that knowing the CS tensor orientation in the molecular frame becomes crucial for properly interpreting the observed tensor components and their relationships to chemical bonding. The observed $\delta_{11}-\delta_{22}$ "cross-over" effects can be readily explained on the basis of a major quinone-type resonance structure of the phenolate anion. The observed sensitivity of ^{17}O CS tensor components toward phenol ionization makes it possible to use solid-state ^{17}O NMR as a new probe for monitoring Tyr side chains in proteins.

Acknowledgment. This work was supported by the Natural Sciences and Engineering Research Council (NSERC) of Canada. Quantum chemical calculations were performed at the High Performance Computing Virtual Laboratory (HPCVL) at Queen's University. Access to the 900 MHz NMR spectrometer was provided by the National Ultrahigh Field NMR Facility for Solids (Ottawa, Canada), a national research facility funded by the Canada Foundation for Innovation, the Ontario Innovation Trust, Recherche Québec, the National Research Council Canada, and Bruker BioSpin and managed by the University of Ottawa (www.nmr900.ca). NSERC is acknowledged for a Major Resources Support grant. We are grateful to Dr. Eric Ye for assistance in acquiring some of the solid-state ^{17}O NMR spectra at 21.14 T and to Dr. Victor Terskikh for assistance with CASTEP calculations.

Supporting Information Available: ^{13}C CP/MAS spectra of L-Tyr and L-TyrHCl, ^{17}O NMR titration data, and fully geometry optimized structures of phenol and phenolate. This material is available free of charge via the Internet at http://pubs.acs.org.

References and Notes

(1) Lemaître, V.; Smith, M. E.; Watts, A. *Solid State Nucl. Magn. Reson.* **2004**, *26*, 215–235.
(2) Wu, G. *Prog. Nucl. Magn. Reson. Spectrosc.* **2008**, *52*, 118–169.
(3) Dong, S.; Yamada, K.; Wu, G. *Z. Naturforsch., A* **2000**, *55*, 21–28.
(4) Zhang, Q.; Chekmenev, E. Y.; Wittebort, R. J. *J. Am. Chem. Soc.* **2003**, *125*, 9140–9146.
(5) Wu, G.; Yamada, K. *Solid State Nucl. Magn. Reson.* **2003**, *24*, 196–208.
(6) Wong, A.; Pike, K. J.; Jenkins, R.; Clarkson, G. J.; Anupõld, T.; Howes, A. P.; Crout, D. H. G.; Samoson, A.; Dupree, R.; Smith, M. E. *J. Phys. Chem. A* **2006**, *110*, 1824–1835.
(7) Wu, G.; Dong, S. *J. Am. Chem. Soc.* **2001**, *123*, 9119–9125.
(8) Lemaître, V.; Pike, K. J.; Watts, A.; Anupõld, T.; Samoson, A.; Smith, M. E.; Dupree, R. *Chem. Phys. Lett.* **2003**, *371*, 91–97.
(9) Pike, K. J.; Lemaître, V.; Kukol, A.; Anupõld, T.; Samoson, A.; Howes, A. P.; Watts, A.; Smith, M. E.; Dupree, R. *J. Phys. Chem. B* **2004**, *108*, 9256–9263.
(10) Howes, A. P.; Anupõld, T.; Lemaître, V.; Kukol, A.; Watts, A.; Samoson, A.; Smith, M. E.; Dupree, R. *Chem. Phys. Lett.* **2006**, *421*, 42–46.
(11) Wong, A.; Howes, A. P.; Pike, K. J.; Lemaître, V.; Watts, A.; Anupõld, T.; Past, J.; Samoson, A.; Dupree, R.; Smith, M. E. *J. Am. Chem. Soc.* **2006**, *128*, 7744–7745.
(12) Yamada, K.; Shimizu, T.; Tansho, M.; Nemoto, T.; Asanuma, M.; Yoshida, M.; Yamazaki, T.; Hirota, H. *Magn. Reson. Chem.* **2007**, *45*, 547–556.
(13) Yamada, K.; Shimizu, T.; Ohki, S.; Yamazaki, T. *Magn. Reson. Chem.* **2008**, *46*, 226–234.
(14) Yamauchi, K.; Kuroki, S.; Ando, I.; Ozaki, T.; Shoji, A. *Chem. Phys. Lett.* **1999**, *302*, 331–336.
(15) Lemaître, V.; De Planque, M. R. R.; Howes, A. P.; Smith, M. E.; Dupree, R.; Watts, A. *J. Am. Chem. Soc.* **2004**, *126*, 15320–15321.
(16) Hu, J.; Chekmenev, E. Y.; Gan, Z.; Gor'kov, P. L.; Saha, S.; Brey, W. W.; Cross, T. A. *J. Am. Chem. Soc.* **2005**, *127*, 11922–11923.
(17) Waddell, K. W.; Chekmenev, E. Y.; Wittebort, R. J. *J. Phys. Chem. B* **2006**, *110*, 22935–22941.
(18) Chekmenev, E. Y.; Waddell, K. W.; Hu, J.; Gan, Z.; Wittebort, R. J.; Cross, T. A. *J. Am. Chem. Soc.* **2006**, *128*, 9849–9855.
(19) Gullion, T.; Yamauchi, K.; Okonogi, M.; Asakura, T. *Macromolecules* **2007**, *40*, 1363–1365.
(20) Wu, G.; Dong, S.; Ida, R. *Chem. Commun.* **2001**, 891–892.
(21) Wu, G.; Dong, S.; Ida, R.; Reen, N. *J. Am. Chem. Soc.* **2002**, *124*, 1768–1777.
(22) Hung, I.; Uldry, A.-C.; Becker-Baldus, J.; Webber, A. L.; Wong, A.; Smith Mark, E.; Joyce, S. A.; Yates, J. R.; Pickard, C. J.; Dupree, R.; Brown, S. P. *J. Am. Chem. Soc.* **2009**, *131*, 1820–1834.
(23) Kwan, I. C. M.; Mo, X.; Wu, G. *J. Am. Chem. Soc.* **2007**, *129*, 2398–2407.
(24) Wu, G.; Yamada, K.; Dong, S.; Grondey, H. *J. Am. Chem. Soc.* **2000**, *122*, 4215–4216.
(25) Yamada, K.; Dong, S.; Wu, G. *J. Am. Chem. Soc.* **2000**, *122*, 11602–11609.
(26) Dong, S.; Ida, R.; Wu, G. *J. Phys. Chem. A* **2000**, *104*, 11194–11202.
(27) Scheubel, W.; Zimmermann, H.; Haeberlen, U. *J. Magn. Reson.* **1985**, *63*, 544–555.
(28) Wu, G.; Mason, P.; Mo, X.; Terskikh, V. *J. Phys. Chem. A* **2008**, *112*, 1024–1032.
(29) Zhu, J.; Geris, A. J.; Wu, G. *Phys. Chem. Chem. Phys.* **2009**, *11*, 6972–6980.
(30) Sefzik, T. H.; Houseknecht, J. B.; Clark, T. M.; Prasad, S.; Lowary, T. L.; Gan, Z.; Grandinetti, P. J. *Chem. Phys. Lett.* **2007**, *434*, 312–315.
(31) Wu, G.; Zhu, J.; Mo, X.; Wang, R. Y.; Terskikh, V. *J. Am. Chem. Soc.* **2010**, *132*, 5143–5155.
(32) Zhu, J.; Ye, E.; Terskikh, V.; Wu, G. *Angew. Chem., Int. Ed.* [Online early access]. DOI: 10.1002/anie.201002041. Published Online: Jul 29, **2010**.
(33) Dollinger, G.; Eisenstein, L.; Lin, S.-L.; Nakanishi, K.; Termini, J. *Biochemistry* **1986**, *25*, 6524–6533.
(34) Roepe, P. D.; Ahl, P. L.; Herzfeld, J.; Lugtenburg, J.; Rothschild, K. J. *J. Biol. Chem.* **1988**, *263*, 5110–5117.
(35) Harada, I.; Yamagishi, T.; Uchida, K.; Takeuchi, H. *J. Am. Chem. Soc.* **1990**, *112*, 2443–2445.
(36) Atkins, W. M.; Wang, R. W.; Bird, A. W.; Newton, D. J.; Lu, A. Y. H. *J. Biol. Chem.* **1993**, *268*, 19188–19191.
(37) Sackett, D. L.; Ruvinov, S. B.; Thompson, J. *Protein Sci.* **1999**, *8*, 2121–2129.
(38) Sonar, S.; Lee, C.-P.; Coleman, M.; Patel, N.; Liu, X.; Marti, T.; Gobind Khorana, H.; RajBhandary, U. L.; Rothschild, K. J. *Nat. Struct. Biol.* **1994**, *1*, 512–517.
(39) Tremmel, S.; Beyermann, M.; Oschkinat, H.; Bienert, M.; Naumann, D.; Fabian, H. *Angew. Chem., Int. Ed.* **2005**, *44*, 4631–4635.
(40) Harada, I.; Yamagishi, T.; Uchida, K.; Takeuchi, H. *J. Am. Chem. Soc.* **1990**, *112*, 2443–2445.
(41) Wilbur, D. J.; Allerhand, A. *J. Biol. Chem.* **1976**, *251*, 5187–5194.
(42) Howarth, O. W.; Lilley, D. M. *Prog. Nucl. Magn. Reson. Spectrosc.* **1978**, *12*, 1–40.
(43) Kato-Toma, Y.; Iwashita, T.; Masuda, K.; Oyama, Y.; Ishiguro, M. *Biochem. J.* **2003**, *371*, 175–181.
(44) Norton, R. S.; Bradbury, J. H. *J. Chem. Soc., Chem. Commun.* **1974**, 870–871.
(45) Herzfeld, J.; Das Gupta, S. K.; Farrar, M. R.; Harbison, G. S.; McDermott, A. E.; Pelletier, S. L.; Raleigh, D. P.; Smith, S. O.; Winkel, C.; Lugtenburg, J.; Griffin, R. G. *Biochemistry* **1990**, *29*, 5567–5574.
(46) De Groot, H. J. M.; Raap, J.; Winkel, C.; Hoff, A. J.; Lugtenburg, J. *Chem. Phys. Lett.* **1990**, *169*, 307–310.
(47) Eckert, H.; Fiat, D. *Int. J. Pept. Protein Res.* **1986**, *27*, 613–616.
(48) Gerothanassis, I. P.; Birlirakis, N.; Sakarellos, C.; Marraud, M. *J. Am. Chem. Soc.* **1992**, *114*, 9043–9047.
(49) Boykin, D. W.; Baumstark, A. L.; Beeson, M. *J. Org. Chem.* **1991**, *56*, 1969–1971.
(50) Brinkmann, A.; Kentgens, A. P. M. *J. Phys. Chem. B* **2006**, *110*, 16089–16101.
(51) Gervais, C.; Dupree, R.; Pike, K. J.; Bonhomme, C.; Profeta, M.; Pickard, C. J.; Mauri, F. *J. Phys. Chem. A* **2005**, *109*, 6960–6969.
(52) Gullion, T. *J. Magn. Reson., Ser. A* **1995**, *117*, 326–329.

(53) Goldbourt, A.; Vega, S.; Gullion, T.; Vega Alexander, J. *J. Am. Chem. Soc.* **2003**, *125*, 11194–11195.
(54) Brinkmann, A.; Kentgens, A. P. M. *J. Am. Chem. Soc.* **2006**, *128*, 14758–14759.
(55) Ye, C.; Fu, R.; Hu, J.; Ding, S. *Magn. Reson. Chem.* **1993**, *31*, 699–704.
(56) Ohgo, K.; Niemczura, W. P.; Kumashiro, K. K. *Macromolecules* **2009**, *42*, 7024–7030.
(57) Eichele, K.; Wasylishen, R. E. *WSOLIDS1: Solid-State NMR Simulations*, version 1.19.11 ed.; Dalhousie University: Halifax, Canada, 2009.
(58) Massiot, D.; Fayon, F.; Capron, M.; King, I.; Le Calve, S.; Alonso, B.; Durand, J.-O.; Bujoli, B.; Gan, Z.; Hoatson, G. *Magn. Reson. Chem.* **2002**, *40*, 70–76.
(59) Segall, M. D.; Lindan, P. J. D.; Probert, M. J.; Pickard, C. J.; Hasnip, P. J.; Clark, S. J.; Payne, M. C. *J. Phys.: Condens. Matter* **2002**, *14*, 2717–2744.
(60) Profeta, M.; Mauri, F.; Pickard, C. J. *J. Am. Chem. Soc.* **2003**, *125*, 541–548.
(61) Frey, M. N.; Koetzle, T. F.; Koetzle, F.; Lehmann, M. S.; Hamilton, W. C. *J. Chem. Phys.* **1973**, *58*, 2547–2556.
(62) Te Velde, G.; Bickelhaupt, F. M.; Baerends, E. J.; Fonseca Guerra, C.; Van Gisbergen, S. J. A.; Snijders, J. G.; Ziegler, T. *J. Comput. Chem.* **2001**, *22*, 931–967.
(63) Vosko, S. H.; Wilk, L.; Nusair, M. *Can. J. Phys.* **1980**, *58*, 1200–1211.
(64) Perdew, J. P.; Burke, K.; Ernzerhof, M. *Phys. Rev. Lett.* **1996**, *77*, 3865–3868.
(65) Schreckenbach, G.; Ziegler, T. *Int. J. Quantum Chem.* **1997**, *61*, 899–918.
(66) van Lenthe, E.; Baerends, E. J.; Snijders, J. G. *J. Chem. Phys.* **1993**, *99*, 4597–4610.
(67) van Lenthe, E.; Baerends, E. J.; Snijders, J. G. *J. Chem. Phys.* **1994**, *101*, 9783–9792.
(68) van Lenthe, E.; Snijders, J. G.; Baerends, E. J. *J. Chem. Phys.* **1996**, *105*, 6505–6516.
(69) Van Lenthe, E.; Van Leeuwen, R.; Baerends, E. J.; Snijders, J. G. *Int. J. Quantum Chem.* **1996**, *57*, 281–293.
(70) Pyykko, P. *Mol. Phys.* **2001**, *99*, 1617–1629.
(71) Wasylishen, R. E.; Bryce, D. L. *J. Chem. Phys.* **2002**, *117*, 10061–10066.
(72) Shannon, R. D. *Acta Crystallogr., Sect. A* **1976**, *A32*, 751–767.
(73) Morgan, K. R.; Newman, R. H. *J. Am. Chem. Soc.* **1990**, *112*, 4–7.
(74) Frydman, L.; Chingas, G. C.; Lee, Y. K.; Grandinetti, P. J.; Eastman, M. A.; Barrall, G. A.; Pines, A. *Isr. J. Chem.* **1992**, *32*, 161–164.
(75) de Dios, A. C.; Laws, D. D.; Oldfield, E. *J. Am. Chem. Soc.* **1994**, *116*, 7784–7786.
(76) Chen, X.; Zhan, C.-G. *J. Mol. Struct.* **2004**, *682*, 73–82.
(77) Portalone, G.; Schultz, G.; Domenicano, A.; Hargittai, I. *Chem. Phys. Lett.* **1992**, *197*, 482–488.
(78) Larsen, N. W. *J. Mol. Struct.* **1979**, *51*, 175–190.
(79) Ramsey, N. F. *Phys. Rev.* **1950**, *78*, 699–703.
(80) Jameson, C. J.; Gutowsky, H. S. *J. Chem. Phys.* **1964**, *40*, 1714–1724.
(81) Flygare, W. H.; Lowe, J. T. *J. Chem. Phys.* **1965**, *43*, 3645–3653.
(82) Flygare, W. H.; Weise, V. W. *J. Chem. Phys.* **1966**, *45*, 2785–2792.
(83) Zilm, K. W.; Grant, D. M. *J. Am. Chem. Soc.* **1981**, *103*, 2913–2922.
(84) Wu, G.; Lumsden, M. D.; Ossenkamp, G. C.; Eichele, K.; Wasylishen, R. E. *J. Phys. Chem.* **1995**, *99*, 15806–15813.
(85) Kirby, C. W.; Lumsden, M. D.; Wasylishen, R. E. *Can. J. Chem.* **1995**, *73*, 604–613.

JP1055123